

# Human Identification from Body Shape

Afzal Godil, Patrick Grother and Sandy Ressler  
National Institute of standards and Technology, Gaithersburg, MD 20899  
{godil, pgrother, sressler}@nist.gov

## Abstract

*In this paper, we investigate the utility of static anthropometric distances as a biometric for human identification. The 3D landmark data from the CAESAR database is used to form a simple biometric consisting of distances between fixed rigidly connected body locations. This biometric is overt, and invariant to view and body posture. We use this to quantify the asymmetry of human bodies, and to characterize the interpersonal and intrapersonal distance distributions. The former is computed directly and the latter by adding zero-mean gaussian noise to the landmark points. This simulation framework is applicable to arbitrary shape based biometrics. We use gross body proportions information to model a computer vision recognition system.*

## 1. Introduction

Humans can be classified by biometric shape information. Systems based on hand geometry and 3D face information have been studied and deployed. The performance of such biometric systems is measured empirically without explicitly measuring the available information contained in the biometrics. We demonstrate here that the newly available CAESAR database [1,2] may be used to assess the efficacy of shape-based biometrics. We use a small amount of non-dynamic anthropometric information to examine how well a hypothetical computer vision system would perform at human identification. The CAESAR database provides a perfect corpus for this study because it contains high resolution, three-dimensional, shape information for a large population.

For our study, we selected from the seventy-three CAESAR anthropometric landmarks those points that yield overtly visible inter-joint distances. We use those 3433 bodies for which the CAESAR database lists no problems and no missing data. We use the FRVT 2002 methodology [3,4]: we form gallery and probe sets and

compute a distance matrix that quantifies the closeness of the 3433 persons in the sets. We compute recognition performance for a system based on static body shape. The result can be used as a baseline for gait algorithms designed to exploit kinematic information [6,7,8].

The next section details the CAESAR database. Section 3 presents an elementary but viable biometric formed from static information. Section 4 shows the effect of measurement error, and examines human asymmetry. Finally, we present identification and verification performance scores.

## 2. CAESAR database

The CAESAR (Civilian American and European Surface Anthropometry Resource) project has collected 3D Scans, seventy-three Anthropometry Landmarks, and Traditional Measurements data of 5000 people. The objective of this study was to represent, in three-dimensions, the anthropometric variability of the civilian populations of Europe and North America. The CAESAR project employs both 3-D scanning and traditional tools for body measurements for people ages 18-65. A typical CAESAR body is shown in Figure 1.



Figure 1. A typical Caesar body and the landmark points

The seventy-three Anthropometry Landmarks were extracted from the scans. These are point-to-point distances where the points are pre-marked by pasting small stickers on the body and automatically extracted using landmark software. The landmarks identify key bone joint structure and are adequate to segment the body and produce anatomical reference axis systems for the key body segments and joints. The available landmarks are listed in Table 1.

Table 1. Numbers and name of the Landmark Points, arranged in point-picking order

1 Sellion	37 Rt. Metacarpal Phal. II
2 Rt. Infraorbitale	38 Rt. Dactylion
3 Lt. Infraorbitale	39 Rt. Ulnar Styloid
4 Supramenton	40 Rt. Metacarpal-Phal. V
5 Rt. Tragion	41 Lt. Acromion
6 Rt. Gonion	42 Lt. Axilla, Ant
7 Lt. Tragion	43 Lt. Radial Styloid
8 Lt. Gonion	44 Lt. Axilla, Post.
9 Nuchale	45 Lt. Olecranon
10 Rt. Clavicale	46 Lt. Humeral Lateral Epicon
11 Suprasternale	47 Lt. Humeral Medial Epicon
12 Lt. Clavicale	48 Lt. Radiale
13 Rt. Thelion/Bustpoint	49 Lt. Metacarpal-Phal. II
14 Lt. Thelion/Bustpoint	50 Lt. Dactylion
15 Substernale	51 Lt. Ulnar Styloid
16 Rt. 10th Rib	52 Lt. Metacarpal-Phal. V
17 Rt. ASIS	53 Rt. Knee Crease
18 Lt. 10th Rib	54 Rt. Femoral Lateral Epicon
19 Rt. Iliocristale	55 Rt. Femoral Medial Epicon
21 Rt. Trochanterion	56 Rt. Metatarsal-Phal. V
22 Lt. Iliocristale	57 Rt. Lateral Malleolus
23 Lt. Trochanterion	58 Rt. Medial Malleolus
24 Cervicale	59 Rt. Sphyrion
25 10th Rib Midspine	60 Rt. Metatarsal-Phal. I
26 Rt. PSIS	61 Rt. Calcaneus, Post.
27 Lt. PSIS	62 Rt. Digit II
28 Waist, Preferred, Post.	63 Lt. Knee Crease
29 Rt. Acromion	64 Lt. Femoral Lateral Epicon
30 Rt. Axilla, Ant	65 Lt. Femoral Medial Epicon
31 Rt. Radial Styloid	66 Lt. Metatarsal-Phal. V
32 Rt. Axilla, Post.	67 Lt. Lateral Malleolus
33 Rt. Olecranon	68 Lt. Medial Malleolus
34 Rt. Humeral Lateral Epicon	69 Lt. Sphyrion
35 Rt. Humeral Medial Epicon	70 Lt. Metatarsal-Phal. I
36 Rt. Radiale	71 Lt. Calcaneus, Post.
	72 Lt. Digit II
	73 Crotch

### 3. Body Shape as Biometric

The landmark points on the human body as shown in Figure 2, are located on the surface of the CAESAR body. Assuming a Cartesian coordinate system, the  $i$ -th landmark point is  $P_i = (x_i, y_i, z_i)$ . The CAESAR database provides seventy-three such points for the 5000 subjects, in the three poses. For recognition purposes, we require

only those points where their separations are pose-independent and feasibly findable in a camera's field of view. This applies to points connected by a single large bone. Thus, we form a biometric vector of twelve distances,  $\mathbf{d}$ , with  $d_1$  wrist to elbow,  $d_2$ , elbow to shoulder,  $d_3$  hip to knee etc. for which the Euclidean distance  $d = \|P_i - P_j\|$  is invariant across different poses. Distances such as chin-knee are avoided. All measurements are in millimeters (mm).

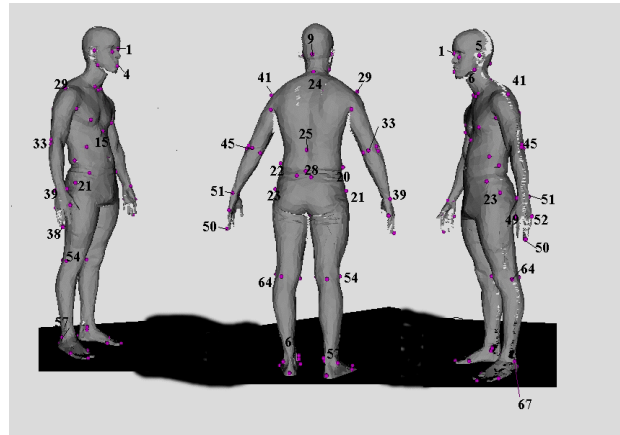


Figure 2. A typical Caesar body and the landmark numbers and positions

### 4 The Error Modeling

A computer vision based system will incur some error in measurement of the landmark points. This actual error is a complex function of the imaging system, image post-processing, and 3D calculation algorithm. For simplicity, we avoid any analysis of this process, instead specify an equivalent error on the position of the landmarks, and study the effect of error on the recognizer.

Because the CAESAR database contains high quality measurements which essentially define the ground truth and does not contain second measurements of each person, we model subsequent appearances of a person by perturbing the known landmark point  $L_i$  by adding zero mean Gaussian random noise  $N(0, \sigma^2)$  isotropically to each coordinate. The displacement of each point will have a Maxwell distribution of the form

$$f(r, a) = \sqrt{\frac{2}{\pi}} a^{3/2} r^2 e^{-ar^2/2}$$

where  $a = \sigma^{-2}$ , the distance  $r$ , has variance  $\sigma_M^2 = (3\pi - 8)/\pi a$ , and the root mean square perturbation is  $\sqrt{(3/a)}$ . In

our trials when we add noise to each coordinate  $N(0, \sigma^2)$  the effect on distance is shown in Table 2.

Table 2. Gaussian Noise versus Maxwell RMS Displacement

Gaussian Noise $\sigma$ (mm)	Maxwell RMS Displacement (mm)
5	8.66
10	17.32
15	25.98
20	34.64
25	43.3

This noise model is homogenous over persons and landmark points, and isotropic over coordinates. This is clearly the simplest case. A fuller treatment of noise should be considered for other applications and human body parts.

The effect of adding noise to landmark points is shown in Figures 3a, b, and c, which give the distributions of the wrist-elbow distance as the standard deviation of the noise varies from zero to 25 mm. The observed maximum values of the perturbation are within about  $\pm 5\sigma$ .

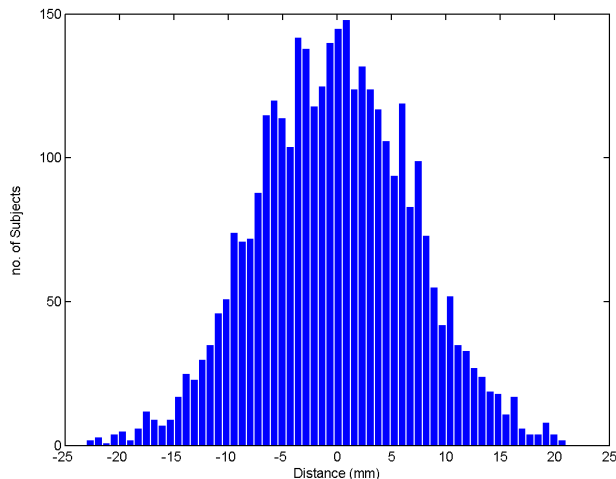


Figure 3a. Histogram of difference in distance between wrists to the elbow at noise level of  $\sigma = 5$  mm.

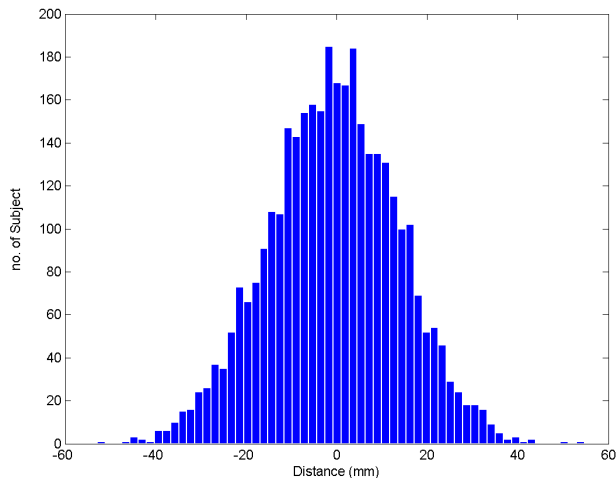


Figure 3b. Histogram of difference in distance between wrists to the elbow at noise level of  $\sigma = 10$  mm.

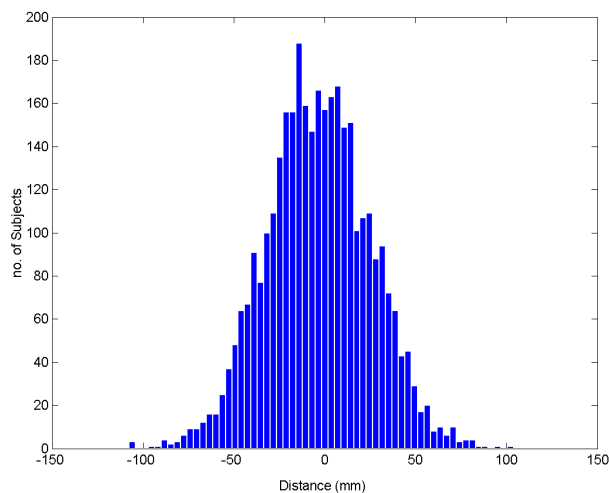


Figure 3c. Histogram of difference in distance between wrists to the elbow at noise level of  $\sigma = 20$  mm.

## 5. The Asymmetry Problem

In this study, we compare the effect of asymmetry in human body and measurement error for biometric evaluation. In this discussion, “gallery” refers to the groups of enrolled biometric signatures and “probe set” refers to the groups of “unknown” test signatures. For the gallery, we use invariant segments from left part of the body and distances from the right side for the probe set.. The recognition engine then simply computes the  $L_1$  distance between all pairs of  $i$ -th gallery and the  $j$ -th probe signatures to form the distance matrix with six, nine, and twelve segments. The total number of subjects

with clean and complete data in landmark points is 3433, and all of those individuals are used in the recognition.

The asymmetry in the distances is shown as a histogram in figures 4a and 4b. The difference in the distances between the left and right side for the elbow to wrist and from elbow to shoulder are around 40 mm. The difference is mainly due to measurement error and natural asymmetry in human body.

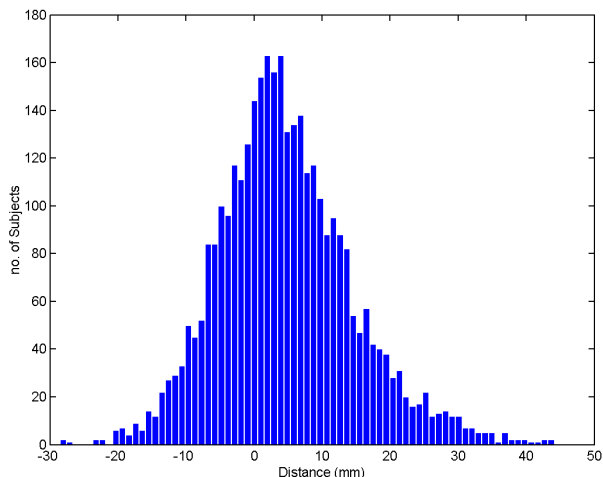


Figure 4a. Histogram of the left-right difference in distance between wrist and elbow

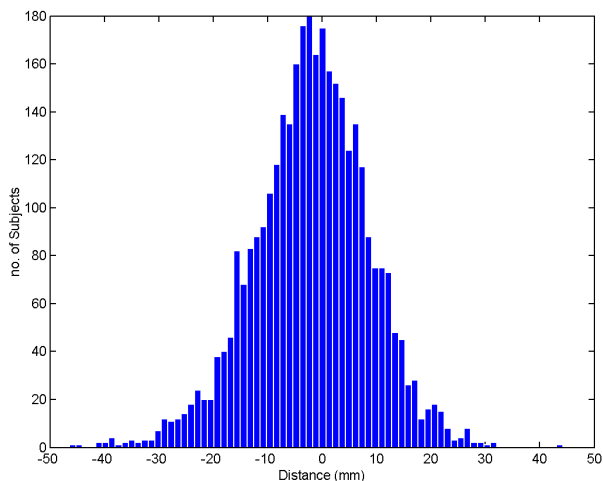


Figure 4b. Histogram of the left-right difference in distance between elbow and shoulder

## 6. Recognition Performance

We have followed the FRVT 2002 [3,4,5] methodology and have simply inserted the original biometric vector  $d$ , from each subject into the gallery and have inserted the noise perturbed vector  $d'$  into the probe set.

The resulting matrices are used to compute the identification and verification performance scores. The standard measure of verification performance is Receiver Operating Characteristic (ROC). The ROC plot shows the false alarm rate (FAR) on the horizontal axis and the probability of verification on the vertical axis, which is also one minus the false reject rate (1-FRR). FAR is the percentage of imposters wrongly accepted by the security system while FRR is the percentage of valid users rejected by the security system. Hence there is tradeoff between FAR and FRR that depends on security policy and through-put requirements.

The measure of identification performance is the “rank order statistics,” called the Cumulative Match Characteristics (CMC). The rank order statistics indicate the probability that the gallery subject will be among the top  $r$  matches to a probe. This probability depends upon both, gallery size  $G$  and  $r$ .

## 7. Results

The results for error modeling and the asymmetry problem are presented in the next two sub sections.

### 7.1. Results for the Error Modeling

The dependence of rank one identification performance,  $CMC(1)$ , on gallery size  $G$  is of primary concern and is shown in Figure 5. For a noise of  $\sigma = 10$  mm, the  $CMC(1)$  at a gallery size of 3433 drops to 0.2.

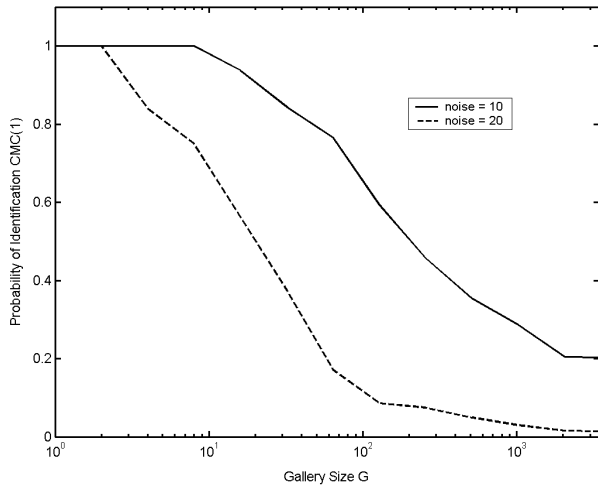


Figure 5. Effect of population size. As gallery size  $G$  increases, the rank one identification rate falls rapidly.

An Identification Performance based on Cumulative Match Characteristic and different level of noise added is shown as a Boxplot in Figure 6. The plot shows the probability of matching the gallery subject at the top 1 rank vs. the noise level. The probability of match at 1 rank is 100% at 0 mm noise level, drops to 45% at noise level of  $\sigma = 7.5\text{mm}$  and 20% at the noise level of  $\sigma = 10\text{mm}$ .

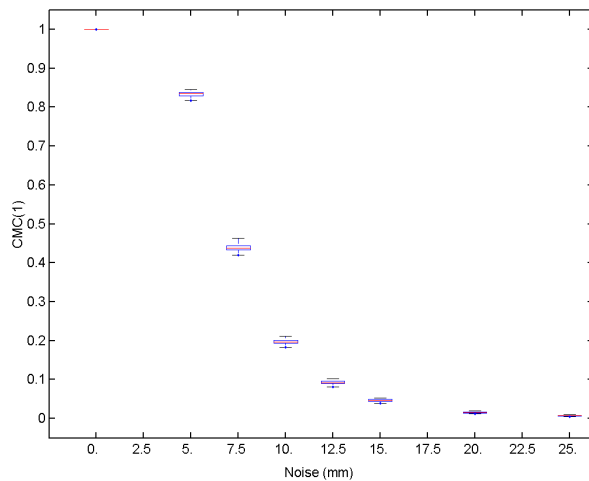


Figure 6. Boxplot of the Cumulative Match Characteristics at Rank 1 versus location perturbation in mm.

In Figure 7 we see the Cumulative Match Characteristics for the twelve element biometric signature degraded by increasing amounts of location perturbation noise. The curves exhibit the usual rise, approaching 1 as the rank

approaches the gallery size. For large amounts of noise the population is essentially unidentifiable using this biometric. The same finding is evident in the verification ROCs of Figure 8.

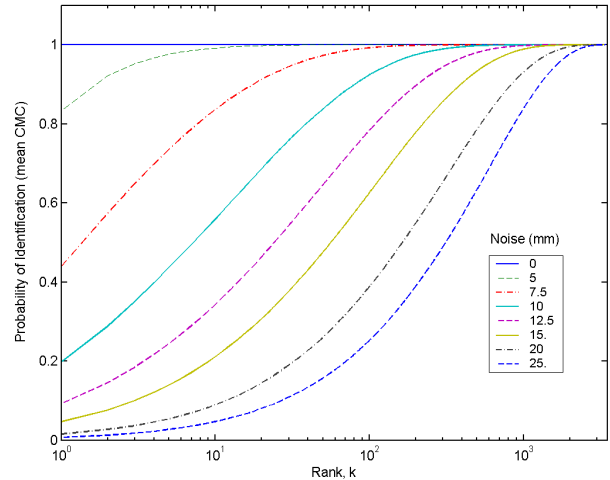


Figure 7. Identification performance, plotted as CMC, shows effect of rank for different noise levels.

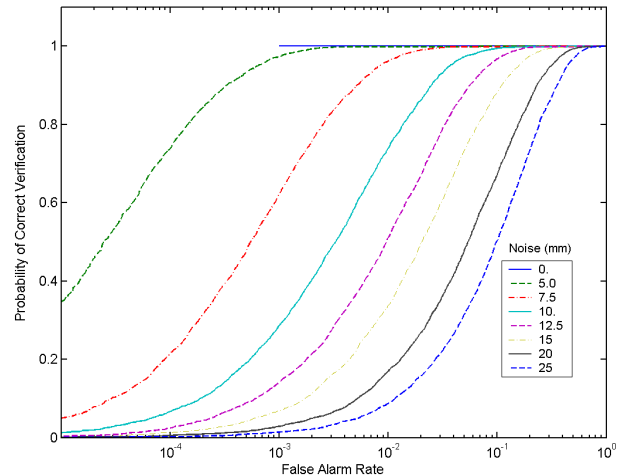


Figure 8. Verification performance, plotted as ROCs, for increasing location perturbation values.

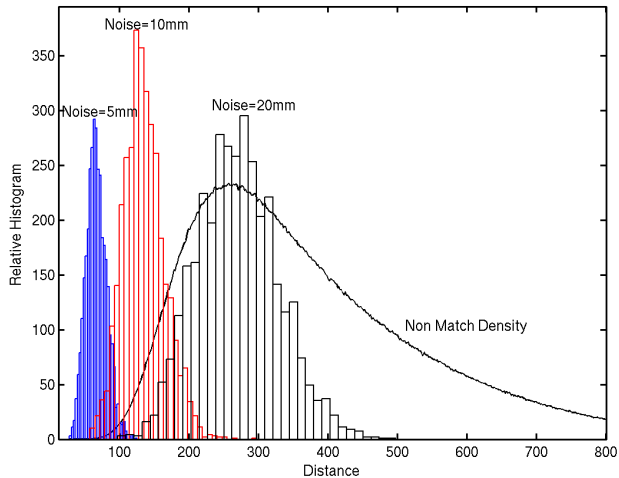


Figure 9. The match and non-match densities.

Figure 9 shows the match and non-match densities for noise levels of  $\sigma=5, 10,$  and  $20$  mm. As the noise level is increased, the match and non-match distributions overlap leading to decreased recognition performance.

## 7.2. Results for the Asymmetry Problem

The dependency of CMC(1) on gallery size for the asymmetry problem is shown in Figure 10, for a gallery size of 3433, the CMC(1) drops to 0.4

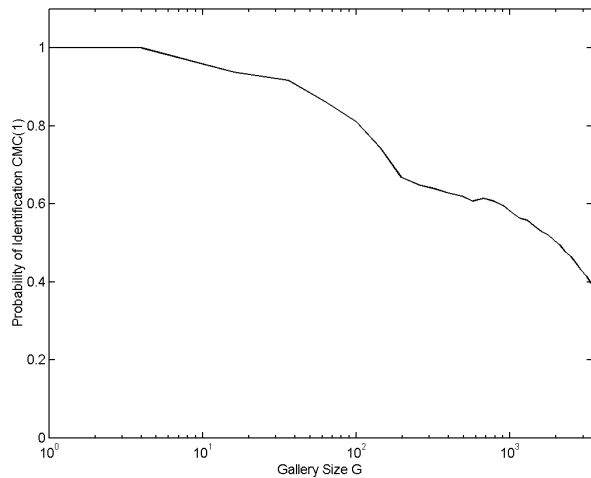


Figure 10. Effect of gallery size for left-right asymmetry signatures

The evaluation performed on the data based on two metrics, Identification Performance based on Cumulative Match Characteristic is shown in Figure 11. The plot shows the fractions of probe signatures whose gallery match was within the given ranks. This is plotted for signatures containing six, nine and twelve segments.

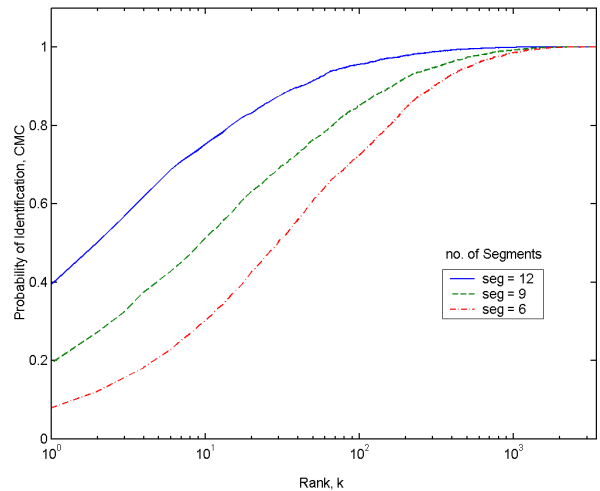


Figure 11. The Cumulative Match Characteristic curves for the Asymmetry Problem for Different Number of Segments

Next we show verification performance of the biometric using the Receiver Operating Characteristics (ROC) as shown Figure 12. The ROC graph shows the true accept rate (legitimate access) vs. the false accept rate (erroneous admission) and shows that as the number of elements of the biometric signature is increased a person becomes more left-right self-similar. With 12 elements 80% of persons are correctly verified while falsely accepting 1%.

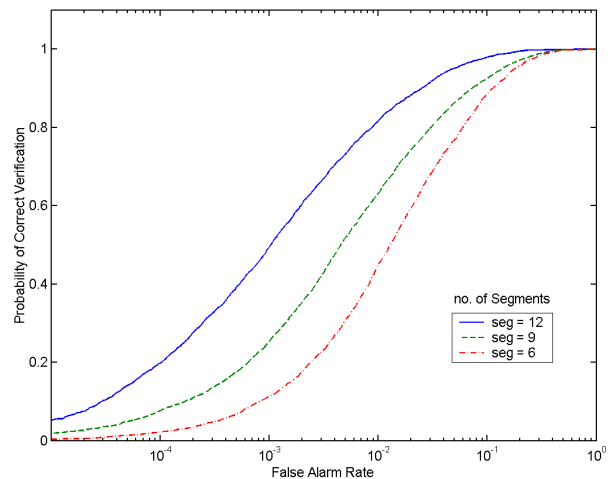


Figure 12. ROC curve for six, nine, and twelve segments for the asymmetry problem.

## 8. Conclusion

We have simulated a computer vision identification system that attempts to recognize humans from their overt static body measurements. We have shown, via a simple biometric of twelve static body measurements, that the viability of a biometric can be measured by synthetically degrading it. We acknowledge that the noise model is important to comparing the result with samples drawn from the interpersonal non-match.

The simple biometric signature we defined, performs poorly except when the match distribution is only minimally degraded. Two means of improving such an identification system are to use a richer set of overt body distances, and to reduce localization errors. The former requires a more sophisticated computer vision system. The later should be realizable if, given a video sequence instead of a single snapshot, the positional errors can be reduced by coherent averaging through time. Of course video sequences offer temporal information that is employed by dynamical gait recognition algorithms, for example [9].

## 9. References

[1] CAESAR web site  
<http://www.sae.org/technicalcommittees/caesumm.htm>

[2] Civilian American and European Surface Anthropometry Resource (CAESAR) web site  
<http://www.hec.af.mil/cardlab/CAESAR/index.html>

[3] P. Phillips, P. Grother, R. Micheals, D. Blackburn, E. Tabassi and M. Bone "Face Recognition Vendor Test 2002" In NIST Technical Report, NIST IR 6965, March 2003.

[4] S. Rizvi, P. Phillips and H. Moon "The FERET Verification Testing Protocol for Face" In NIST Technical Report, NIST IR 6281, October 1998.

[5] P. Phillips, H. Moon, S. Rizvi, and P. Rauss "The FERET Evaluation Methodology for Face-Recognition Algorithms" In IEEE Trans. Pattern Analysis and Machine Intelligence, 22:1090-1103, 2000.

[6] B. Johnson "Gait recognition using static activity-specific parameters" In Proceedings of Computer Vision and Pattern Recognition Conference (CVPR 2001), Kauai, Hawaii, December 2001.

[7] J. Bobick "A Multi-view Method for Gait Recognition Using Static Body Parameters" In 3rd International Conference on Audio- and Video Based Biometric Person Authentication, pages 301-311, Halmstad, Sweden, June 2001.

[8] C. BenAbdelkader, R. Cutler, and L. Davis "View-invariant Estimation of Height and Stride for Gait Recognition" In Workshop on Biometric Authentication ECCV 2002, Copenhagen, Denmark, June 2002.

[9] A. Sunderesan, A. Chowdhury, R. Chellappa "A HMM Based Framework for Recognition of Humans From Gait Sequences" In IEEE Intl. Conf. on Image Processing, 2003.